

See discussions, stats, and author profiles for this publication at: <https://www.researchgate.net/publication/231667511>

# Charge Transfer between Metal Clusters and Growing Carbon Structures in Chirality-Controlled Single-Walled Carbon Nanotube Growth

ARTICLE *in* JOURNAL OF PHYSICAL CHEMISTRY LETTERS · APRIL 2011

Impact Factor: 7.46 · DOI: 10.1021/jz200417b

---

CITATIONS

13

READS

43

## 5 AUTHORS, INCLUDING:



[Qiang Wang](#)

Nanjing University of Technology

23 PUBLICATIONS 175 CITATIONS

[SEE PROFILE](#)



[Shuo-Wang Yang](#)

Agency for Science, Technology and Research...

41 PUBLICATIONS 656 CITATIONS

[SEE PROFILE](#)



[Yuan Chen](#)

University of Sydney

126 PUBLICATIONS 3,692 CITATIONS

[SEE PROFILE](#)

# Charge Transfer between Metal Clusters and Growing Carbon Structures in Chirality-Controlled Single-Walled Carbon Nanotube Growth

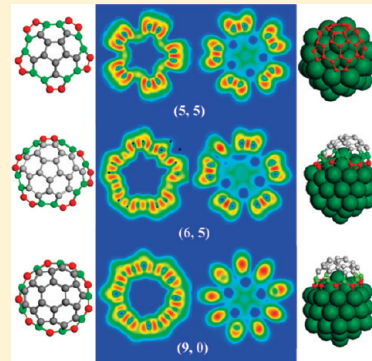
Qiang Wang,<sup>†</sup> Shuo-Wang Yang,<sup>‡</sup> Yanhui Yang,<sup>†</sup> Mary B. Chan-Park,<sup>†</sup> and Yuan Chen<sup>\*†</sup>

<sup>†</sup>School of Chemical and Biomedical Engineering, Nanyang Technological University, 62 Nanyang Drive, Singapore 637459

<sup>‡</sup>Institute of High Performance Computing, 1 Fusionopolis Way, 16-16 Connexis, Singapore 138632

Supporting Information

**ABSTRACT:** Synthesis of single-walled carbon nanotubes (SWCNTs) with specific chirality has been a great challenge. The detailed role of catalyst clusters in chirality-selective growth of SWCNTs is still unclear. We studied armchair (5,5), chiral (6,5), and zigzag (9,0) nanotube growths on a relaxed Ni<sub>55</sub> cluster. Although adhesion energies and chemical potentials of growing carbon structures only show small differences, charges are evidently transferred (or redistributed) from Ni atoms to the growing end edges of nanotubes, which enhance the reactivity of carbon edges. Different chiral nanotubes exhibit distinct reaction active sites. (5,5) has five identical double-carbon active sites, while (9,0) has nine single-carbon active sites. (6,5) has a kink site with the highest reaction activity. These findings imply that the structures of metal clusters strongly correlate with nanotube growth sites through charge transfer (or redistribution). Potential opportunities exist in enabling (n,m) selective growth by engineering charge transfer between metal clusters and growing carbon structures.



## SECTION: Nanoparticles and Nanostructures

Synthesis of single-walled carbon nanotubes (SWCNTs) with specific chirality has been a great challenge. Experimental studies have shown that metal/metal carbide clusters, the most common catalysts used in synthesis, with various sizes, morphology, and composition may lead to preferential growth of a subset of chiral SWCNTs.<sup>1–5</sup> Metal/metal carbide clusters play important roles in catalyzing conversion of the carbon-containing feedstock, annealing defects of growing nanotubes, prevention of SWCNT closure, terminating of edge dangling bonds, and providing critical carbon density.<sup>6–9</sup> SWCNT nucleation and growth is a complex heterogeneous catalysis process. Various factors, such as metal/metal carbide clusters, substrates, and carbon precursors, interplay dynamically in determining the chirality of SWCNTs.<sup>1–5</sup> Understanding all factors is unlikely feasible by current experimental and theoretical studies. If we can identify and understand critical factors, it would be very useful to further improve chirality-selective SWCNT growth. Theoretical studies have suggested the chirality selectivity could be related to the epitaxial matching between nanotube ends and metal catalyst surface atoms,<sup>10</sup> the adhesion strength between nanotubes and catalyst clusters,<sup>11</sup> and chirality-dependent growth rates obeying the dislocation theory.<sup>12</sup> However, the detailed role of metal clusters in chirality-selective growth of SWCNTs remains elusive.

Recent experimental results indicated that the interface between the carbon cap/tube end edge and metal/metal carbide clusters is active in SWCNT growth.<sup>13–15</sup> Charge or electron

transfer is fundamental for explaining structural stability and reactivity of organometallic and metal cluster species.<sup>16</sup> In general, charge transfer is the intrinsic mechanism behind many chemical reactions. It is a useful tool in understanding and predicting the structural change and chemical reactivity in organometallic chemistry. In this study, on the basis of ab initio calculations, we found that significant charge transfer (or charge redistribution) exists between growing carbon structures and metal clusters. The electronic charges transfer evidently from metal surface atoms to carbon atoms, resulting in negative charges accumulated on edge carbon atoms. In contrast, nonedge carbon atoms gain little charge. More importantly, through frontier electron density distribution analysis, we identified that different chiral SWCNTs have distinct reactive sites at their boundaries with metal clusters. This Letter is to show that SWCNT growth sites may be controlled by metal clusters through charge transfer in the chirality-selective synthesis of SWCNTs.

We studied the growth of armchair (5,5), chiral (6,5), and zigzag (9,0) nanotubes on a relaxed Ni<sub>55</sub> cluster. The (5,5) nanotube was selected because a series of near-armchair nanotubes ((6,5), (7,5), (8,5), and (9,5)), which are most commonly found in chiral-selective SWCNT synthesis,<sup>1–5</sup> can all be derived

**Received:** March 28, 2011

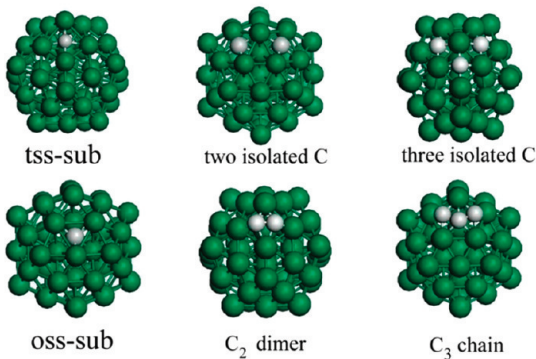
**Accepted:** April 8, 2011

from the (5,5) carbon cap by single carbon atom and C<sub>2</sub> dimer additions.<sup>17</sup> The (6,5) nanotube was chosen as a representative chiral nanotube model. The (9,0) nanotube has a similar diameter as the (5,5) nanotube, while holding a different chiral angle. A high symmetrical icosahedral structure was adopted as an initial structure for the Ni<sub>55</sub> cluster because of the fact that this structure is a local-geometry minimum in its size range. Besides, the Ni<sub>55</sub> cluster has a diameter comparable with that of the armchair (5,5), chiral (6,5), and zigzag (9,0) nanotubes. The Ni<sub>55</sub> cluster has also been often observed in experiments<sup>18,19</sup> and is often used in theoretical studies of SWCNT growth.<sup>11,20,21</sup> All structures, including carbon intermediates C<sub>n</sub>, metal cluster Ni<sub>55</sub>, and Ni<sub>55</sub>-C<sub>n</sub> complexes, are fully relaxed to optimize without any constraints.

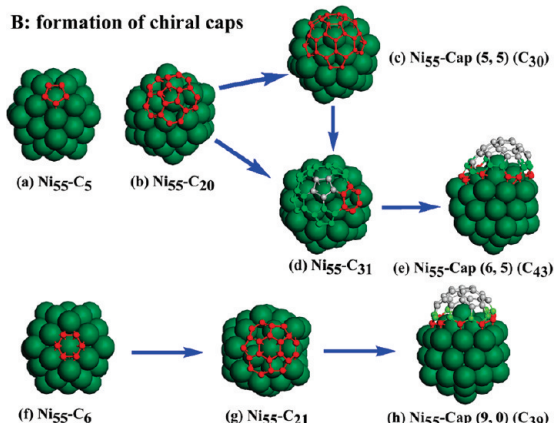
On the basis of the nanotube root growth hypothesis, SWCNT growth on the Ni<sub>55</sub> cluster can be classified into three stages, (1) early nucleation of carbon species (single carbon atom, C<sub>2</sub> dimer, and C<sub>3</sub> chain), (2) formation of (5,5), (6,5), and (9,0) chiral caps from five- and six-membered carbon rings, and (3) continuous growth into (5,5), (6,5), and (9,0) nanotubes. During the initial nucleation stage, carbon species (C, C<sub>2</sub>, and C<sub>3</sub>) may adsorb on different sites of the Ni<sub>55</sub> cluster. They include two stable fcc and hcp three-fold hollow surface sites and two corresponding interstitial subsurface sites, an octahedral (oss) site below the fcc site and a tetrahedral (tss) site below the hcp site. The detailed results of all possible sites for the adsorption of a single carbon atom on various Ni clusters have been discussed in our recent publication.<sup>22</sup> In this study, we extended our study to the nucleation of two or three isolated carbon atoms adsorbed on the Ni<sub>55</sub> cluster, which results in forming C<sub>2</sub> dimers and C<sub>3</sub> chains. A few representative adsorption sites are shown in Figure 1A. The carbon dimer and chain on the Ni<sub>55</sub> cluster would further grow into larger carbon structures.

During the formation of chiral caps and their sequential nanotube growth, it is impractical to calculate all possible Ni<sub>55</sub>-C<sub>n</sub> complexes with different interaction interfaces between C<sub>n</sub> and Ni<sub>55</sub>. A series of representative intermediate structures for the growth of armchair (5,5), chiral (6,5), and zigzag (9,0) nanotubes on the Ni<sub>55</sub> cluster were chosen as studying models. Following the formation of C<sub>2</sub> dimers and C<sub>3</sub> chains, graphitic fragments would evolve into complete carbon caps on the metal cluster by further incorporating C/C<sub>2</sub>. The two pathways, (a) → (c) (the top row of Figure 1B) and (f) → (h) (the bottom row of Figure 1B), illustrate the formation of armchair (5,5) cap and zigzag (9,0) cap, respectively. The (5,5) and (9,0) nanotube each has only one matching chiral cap, which can obey the isolated pentagon rule.<sup>23,24</sup> As illustrated in Figure 1B, the (5,5) cap can be constructed starting from a five-membered carbon ring. Subsequently, 15 carbon atoms were added to the initial five-membered ring to form the intermediate cap fragment (Ni<sub>55</sub>C<sub>20</sub>) (see Figure 1B(b)). Next, the complete (5,5) cap (Ni<sub>55</sub>-(5,5) Cap) was created by joining five C<sub>2</sub> dimers (or 10 carbon atoms) to the intermediate cap fragment Ni<sub>55</sub>C<sub>20</sub> (see Figure 1B(b) and (c)). Similarly, the complete (9,0) cap (Ni<sub>55</sub>-(9,0) Cap) can be built from a six-membered carbon ring, as illustrated in Figure 1B(f)–(h). The formation of (6,5) can be achieved through two paths; 11 carbon atoms can be added to the Ni<sub>55</sub>C<sub>20</sub> to form the intermediate cap fragment Ni<sub>55</sub>C<sub>31</sub> (Figure 1B(b)–(d)), followed by joining six C<sub>2</sub> dimers (or 12 carbon atoms) to have the complete (6,5) cap (Figure 1B(d) and (e)); alternatively, the intermediate cap fragment Ni<sub>55</sub>C<sub>31</sub> can also be formed by a single carbon atom addition to the complete (5,5) cap (Figure 1B(c) and (d)).

### A: initial nucleation



### B: formation of chiral caps



### C: growth of chiral nanotubes

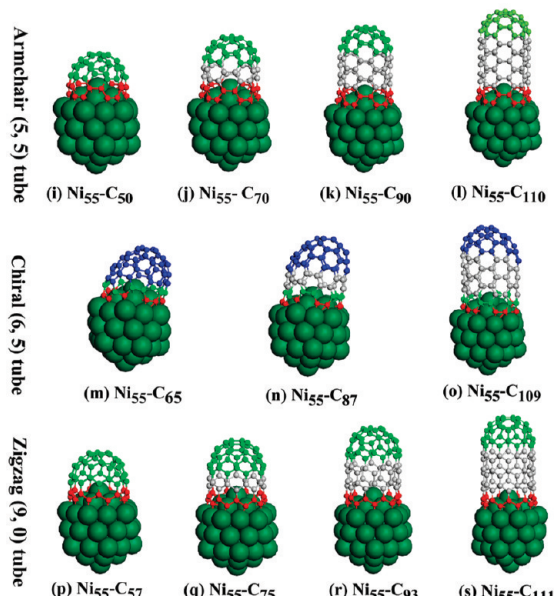


**Figure 1.** On the basis of the carbon nanotube root growth theory, the catalytic growth of armchair (5,5), chiral (6,5), and zigzag (9,0) SWCNTs on the Ni<sub>55</sub> cluster can be classified into three stages, (A) early nucleation of carbon species, such as a single C atom, C<sub>2</sub> dimer, and C<sub>3</sub> chain, (B) formation of (5,5), (6,5), and (9,0) chiral caps from five- or six-membered carbon rings, and (C) continuous growth into (5,5), (6,5), and (9,0) nanotubes, when carbon caps depart from the Ni<sub>55</sub> cluster with certain nanotube lengths.

It has been proposed that a  $(n,m)$  chiral carbon cap can sequentially grow into the corresponding SWCNT with the specific  $(n,m)$  structure by constant addition of carbon atoms.<sup>10,25</sup> In our previous study, we showed that the addition of  $C_2$  dimers at carbon edges of chiral carbon caps can lead to the continuous growth of nanotubes without chirality changes. Moreover,  $n+m$   $C_2$  dimers (the number of a specific  $(n,m)$  tube) are needed to grow one complete ring along the tube edge.<sup>17</sup> Figure 1C illustrates the proposed sequential step-by-step growth of the  $(5,5)$ ,  $(6,5)$ , and  $(9,0)$  chiral caps on the  $Ni_{55}$  cluster. The pathway  $(i) \rightarrow (l)$  (the top row of Figure 1C) represents the growth from the complete  $(5,5)$  cap (Figure 1B(c)) to a short  $(5,5)$  nanotube (Figure 1C(l)) by repeated additions of 10  $C_2$  dimers (or 20 carbon atoms) at the interface between the open edge of the  $(5,5)$  cap/nanotube and the  $Ni_{55}$  cluster. Similarly, the pathway  $(p) \rightarrow (s)$  (the lower row of Figure 1C) represents the growth of a  $(9,0)$  nanotube on the  $Ni_{55}$  cluster from the complete  $(9,0)$  cap (Figure 1B(h)) to the short  $(9,0)$  nanotube (Figure 1C(s)) by repeated additions of nine  $C_2$  dimers (or 18 carbon atoms) to the interface between the open edge of the  $(9,0)$  cap/nanotube and the  $Ni_{55}$  cluster. The middle row of Figure 1C(m)–(o) shows the growth of  $(6,5)$  nanotube by repeated additions of 11  $C_2$  dimers (or 22 carbon atoms).

It should be noted that the models shown in Figure 1 are only representative configurations for the growth of  $(5,5)$ ,  $(6,5)$ , and  $(9,0)$  nanotubes. The actual growth process may be less orderly, with numerous polyyne chains and incomplete carbon rings, which have been shown in recent molecular simulations.<sup>26</sup>

The total adhesion energies between  $Ni_{55}$  and carbon structures ( $C_n$ ), cohesive energies of C–C, and chemical potentials of  $C_n$  at different growth stages are shown in Figures S1, S2, and S3 in the Supporting Information (SI), respectively. We found that at the early nucleation stage, small carbon species (e.g.,  $C$ ,  $C_2$ , and  $C_3$ ) have higher adhesion energies per carbon atom on the relaxed  $Ni_{55}$  cluster (see Figures S1 and S2, SI). With the growth of carbon structures, the C–C cohesive energy becomes stronger, while the C–Ni interaction becomes weaker (see Figure S2, SI), meaning that it is energetically favorable for the forming, lifting-up, and growing of carbon caps on the metal cluster surface. As depicted in Figure 2, the  $C_5$  or  $C_6$  carbon ring formation requires a large surface coverage of carbon species on metal cluster surfaces because of the high chemical potential barriers for incorporating extra carbon atoms at the early nucleation stages. Once these carbon rings are formed, they can spontaneously extend into complete chiral caps. Small carbon species on  $Ni_{55}$  have high chemical potentials (red line in Figure 2), which provide a driving force for the continuous growth of SWCNTs. (Also see Figure S3, SI.)

However, the growth energies of  $(5,5)$ ,  $(6,5)$ , and  $(9,0)$  nanotubes differ by only a couple of eV. Considering the high growth temperature, it implies no strong preference for specific chirality on  $Ni_{55}$ . On the basis of energy calculations, a recent study suggested that free metal clusters are incapable of growing SWCNTs with desired chiralities,<sup>27</sup> which is not in agreement with existing experimental results.<sup>1–5</sup> Environmental transmission electron microscopy observations suggested that the chirality selectivity of SWCNTs is controlled by the dynamic interplay between growing carbon structures and deformed catalyst clusters.<sup>13–15</sup> The  $(n,m)$  structure of a nanotube could be uniquely determined by its corresponding chiral carbon cap interacting with catalyst clusters.<sup>10</sup> Analyzing all of the optimized geometries of  $Ni_{55}–C_n$  complexes in this study, we noticed that

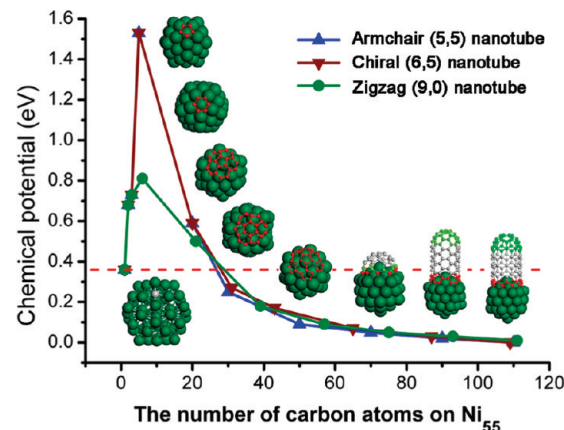


**Figure 2.** Chemical potentials ( $\mu$ ) of  $C_n$  on  $Ni_{55}$  during the growth of  $(5,5)$ ,  $(6,5)$ , and  $(9,0)$  SWCNTs.  $\mu$  is the energy required to add one extra carbon atom to  $C_n$ . The red line indicates the  $\mu$  of C at subsurface octahedral sites of the  $Ni_{55}$  cluster. Some schematic models of the growing  $(5,5)$ ,  $(6,5)$ , and  $(9,0)$  caps and nanotubes are illustrated in the figure.

the relaxed  $Ni_{55}$  cluster and growing carbon structures all deform significantly from their initial structures. The  $Ni_{55}$  cluster deforms from its initial symmetrical icosahedral structure, in particular, at its interface with carbon, in order to match with various end edges of chiral carbon caps. These phenomena suggest that the interface between cap/tube end edges and metal cluster surfaces may have a higher reactivity for SWCNT growth.

We investigated charge transfer between  $C_n$  and  $Ni_{55}$  to better understand hidden roles played by metal clusters. As rendered in Figure S4 (SI), negative charges are transferred (or redistributed) from Ni atoms to carbon atoms when carbon species are absorbed on  $Ni_{55}$ . Inspecting the interfaces of  $Ni_{55}–C_n$  complexes, we found that charges always accumulate on edge carbon atoms; on the contrary, nonedge carbon atoms have little charges (see Figures 3a,c,e,g,i,k and S4, SI). For Ni atoms of  $Ni_{55}$ , charge depletion almost all comes from the carbon neighboring Ni atoms (+0.2 to +0.39 e; see Figure 3b,d,f,h,j,l). Other Ni atoms deplete no charges. These outcomes indicate that the charge transfer/redistribution is short-ranged and mainly occurs between outermost edge carbon atoms and their neighboring Ni atoms.

More importantly, we found that charge distributions at  $Ni_{55}–C_n$  interfaces exhibit specific patterns associated with nanotube chirality. For the armchair  $(5,5)$  cap/nanotube, charges (−0.31 to −0.38 e) mainly accumulate on five pairs of interval outermost edge carbon atoms (red, in Figure 3a,c), while the other edge carbon atoms (green) hardly possess any charge. In contrast, for the zigzag  $(9,0)$  cap/nanotube, charges are localized on nine interval outermost edge carbon atoms (red, in Figure 3i,k), while other edge carbon atoms (green) do not own any charge. For the chiral  $(6,5)$  cap/nanotube, charges mainly accumulate on three carbon atoms (a kink site, red) and four pairs of interval double-carbon atoms (armchair sites, red in Figure 3e,g), while other edge carbon atoms (green) are near-neutral.

The electron localization function (ELF) plots (Figure 4) further illustrate that charges are transferred (or redistributed) evidently from neighboring Ni atoms to edge carbon atoms. Chiral cap/nanotube edges without metal clusters have delocalized  $\pi$ -electrons (Figure 4a,c,e,g,i,k). On the other hand, electrons at  $Ni_{55}–(5,5)$  cap/nanotube interfaces are localized at five pairs of identical edge carbon atoms (Figure 4b,d).

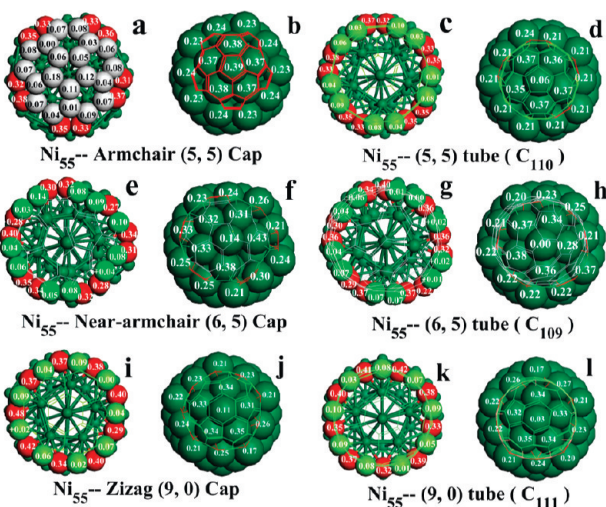


**Figure 3.** Charge distributions of edge carbon atoms (a,c,e,g,i,k) and their corresponding neighboring Ni atoms (b,d,f,h,j,l) on Ni<sub>55</sub>-(S,S) cap (a,b), Ni<sub>55</sub>-(5,5) nanotube (c,d), Ni<sub>55</sub>-(6,5) cap (e,f), Ni<sub>55</sub>-(6,5) nanotube (g,h), Ni<sub>55</sub>-(9,0) cap (i,j), and Ni<sub>55</sub>-(9,0) nanotube (k,l) complexes.

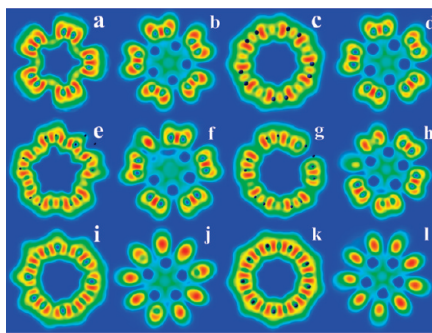


**Figure 4.** ELF plots of edge carbon atoms on C<sub>n</sub> without metal clusters, (a) (5,5) cap, (c) (5,5) nanotube (C<sub>110</sub>), (e) (6,5) cap, (g) (6,5) nanotube (C<sub>109</sub>), (i) (9,0) cap, and (k) (9,0) nanotube (C<sub>111</sub>), and on Ni<sub>55</sub>-C<sub>n</sub> complexes, (b) Ni<sub>55</sub>-(5,5) cap, (d) Ni<sub>55</sub>-C<sub>110</sub>, (f) Ni<sub>55</sub>-(6,5) cap, (h) Ni<sub>55</sub>-C<sub>109</sub>, (j) Ni<sub>55</sub>-(9,0) cap, and (l) Ni<sub>55</sub>-C<sub>111</sub>. The red color indicates higher electron densities.

Moreover, electrons at Ni<sub>55</sub>-(9,0) cap/nanotube interfaces are localized at nine interval carbon atoms (Figure 4j,l), while electrons at Ni<sub>55</sub>-(6,5) cap/nanotube interfaces are at a combination of three carbon atoms of a kink site and four pairs of armchair atoms (Figure 4f,h). The formation of C-Ni bonds significantly disturbs delocalized electron  $\pi$ -conjugation existing at carbon cap/nanotube edges, leading to the loss of their aromaticity.

In order to further understand charge-transfer-induced reactivity, the electron density analysis was performed to determine the electronic density of states (DOS) of edge carbon atoms. According to the frontier orbital theory, reaction sites with higher frontier electron density are more reactive.<sup>28,29</sup> We first compared the electronic DOS of 10 outermost edge carbon atoms with 20 inner carbon atoms on Ni<sub>55</sub>-(5,5) cap (Figure 1B(c)) and Ni<sub>55</sub>-(5,5) nanotube (Figure 1C(l)) complexes. For both the (5,5) cap and nanotube, Figure S6 (SI) indicates that the negative charged outermost edge carbon atoms have significantly higher electron density near the Fermi level than inner carbon

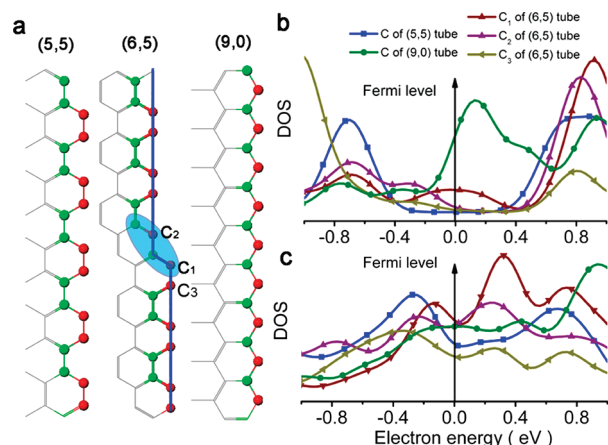


**Figure 5.** (a) Edges of (5,5), (6,5), and (9,0) nanotubes. (b) Electronic DOS of carbon atoms at (5,5), (6,5), and (9,0) nanotube edges without metal clusters and (c) at interfaces between (5,5), (6,5), and (9,0) nanotubes and the Ni<sub>55</sub> cluster.

atoms. It suggests that outermost edge carbon atoms are more reactive than other carbon atoms. This finding agrees with previous published works.<sup>30–32</sup> Outermost edge carbon atoms are the likely reactive sites where SWCNTs can continuously grow by incorporating more carbon atoms. Next, we compared the electronic DOS of edge carbon atoms among (5,5), (6,5), and (9,0) nanotubes. As illustrated in Figure 5a, the edge of the (5,5) nanotube has 10 identical carbon atoms at 5 pairs of armchair sites. Nine identical carbon atoms sit at zigzag sites on the edge of (9,0) nanotube, and the edge of the (6,5) nanotube has three carbon atoms at a kink site and eight carbon atoms at four pairs of armchair sites, similar to the armchair sites of (5,5) nanotube. The electronic DOS of five representative edge carbon atoms (one from (5,5) nanotube, one from (9,0) nanotube, and three from the kink site of (6,5) nanotube) is shown in Figure S7 (SI). The frontier electron density of edge carbon atoms in the Ni<sub>55</sub>-C<sub>n</sub> complexes (Figure S7B, D, and F, SI) is significantly higher than those of carbon atoms at nanotube edges without metal clusters (Figure S7A, C, and E, SI). This can be attributed to charge transfers induced by Ni<sub>55</sub>. It indicates that metal catalysts play an important role in activating nanotube edges.

Furthermore, Figure 5b and c highlights the DOS differences among the three nanotubes. For nanotube edges without metal clusters, carbon atoms on the (9,0) nanotube show higher frontier electron density than carbon atoms on both (5,5) and (6,5) nanotubes. This agrees with the previous work by Kumeda et al., in which they proposed that the zigzag nanotube would grow easier than the armchair nanotube without any catalyst.<sup>30–32</sup> However, due to charge transfer induced by Ni<sub>55</sub>, the carbon atom (C<sub>1</sub>) at the kink site of the (6,5) nanotube possesses higher frontier electron density than carbon atoms at both (9,0) and (5,5) nanotube edges. Because the continuous growth of SWCNTs likely happens at these reactive edge sites through incorporation of additional small carbon species, the more reactive kink site on (6,5) nanotube edges would lead to the preferential growth of chiral (6,5) nanotubes over armchair (5,0) and zigzag (9,0) nanotubes. We hypothesize that these reactive sites are controlled by the structure of Ni<sub>55</sub>.

One long-standing controversy in SWCNT growth research is whether pure metal or metal carbide clusters catalyze the growth

of SWCNTs. Both pure Ni<sup>15</sup> and Fe<sup>33</sup> particles have been observed in the growth SWCNTs. On the other hand, metal carbides, such as Ni<sub>3</sub>C<sup>34</sup> and Fe<sub>3</sub>C<sup>18,35</sup> have also been reported. In general, experimental results have shown that carbon species may dissolve in crystalline metal clusters and supersaturated carbon in the surface area precipitates as graphene.<sup>13–15</sup> In our previous study,<sup>22</sup> we have shown that adsorbed individual carbon atoms on the metal cluster surface can migrate into the underlying interstitial subsurface positions. However, in this study, we found that C<sub>2</sub> and C<sub>3</sub> are unstable at subsurface positions. They would precipitate on the surface and join the growing carbon structure through its active sites. Further work is under way in our lab to understand how metal clusters manage different reactive sites, which includes comparing charge-transfer behaviors at interfaces of various (n,m) nanotubes and pure Ni and Ni carbide clusters, as well as nanotube growth on nonmetal clusters as references. It also should be noted that an alternative approach to achieve chiral-selective growth of SWCNTs is to “clone” nanotubes.<sup>36</sup> Zhang et al. showed that short SWCNTs after removal of –COOH and –OH functional groups can grow under a CH<sub>4</sub> and C<sub>2</sub>H<sub>4</sub> mixture without metal clusters. Moreover, fullerene caps can also be used as seeds for selective growth of SWCNTs.<sup>37</sup> The mechanism of those metal catalyst-free growths could be quite different from that on metal catalysts. The role of charge transfer in such processes requires further investigations.

In conclusion, the growth energies of (5,5), (6,5), and (9,0) nanotubes differ by only a couple of eV, which is not significant considering the high growth temperature. However, charges are transferred (or redistributed) from metal atoms to edge carbon atoms on growing SWCNTs, which enhances the reactivity of edge carbon atoms. Different chiral nanotubes exhibit distinct reaction active sites. The armchair (5,5) nanotube has double-carbon active sites, while the zigzag (9,0) nanotube has single-carbon active sites. The chiral (6,5) nanotube processes a more reactive kink site. These findings imply that the structure of catalytic metal clusters strongly correlates with chiral nanotube growth sites through charge transfer (or redistribution). Therefore, potential opportunities exist in enabling (n,m) selective growth by engineering charge transfer between metal clusters and growing carbon structures.

## ■ COMPUTATIONAL METHODS

Spin-polarized computations were performed with the Perdew–Burke–Ernzerhof (PBE) exchange correlation function<sup>38</sup> using the VASP code.<sup>39,40</sup> The interaction between an atomic core and electrons was described by the projector augmented wave method.<sup>41,42</sup> The plane-wave basis set energy cutoff was set to 400 eV. Periodic boundary conditions were implemented with at least 1 nm of vacuum to preclude interactions between a cluster and its images. Simulation boxes were 20 × 20 × C Å (where C is from 20 to 32 Å) for different calculated systems. The reciprocal space integration was performed with a 1 × 1 × 1 k-point mesh for all calculated systems with discrete characters. All of the structures, including the cluster Ni<sub>55</sub>, carbon intermediates, C<sub>n</sub>, and the complexes Ni<sub>55</sub>–C<sub>n</sub>, were fully relaxed to optimize without any constraint. The global transferred charge was calculated by the atomic Bader charge analysis,<sup>43–45</sup> and the electron distribution was determined by ELF.<sup>46,47</sup>

The chemical potential ( $\mu$ ) of the growing carbon structure (C<sub>n</sub>) on Ni<sub>55</sub>, which is the energy required to add one extra

carbon atom during SWCNT growth, was defined as

$$\mu = \frac{E_{\text{Ni}_{55}-C_n} - E_{\text{Ni}_{55}}}{n} - \mu_C$$

where  $E_{\text{Ni}_{55}-C_n}$  and  $E_{\text{Ni}_{55}}$  are the total energies of fully geometry-optimized complexes with and without C<sub>n</sub>, respectively. Here, n corresponds to the number of carbon atoms in C<sub>n</sub>. The reference chemical potential,  $\mu_C$ , is the chemical potential of a free carbon atom at its ground state, 7.7 eV. The chemical potential has previously been applied in SWCNT nucleation and growth studies.<sup>27</sup>

## ■ ASSOCIATED CONTENT

**S Supporting Information.** Adhesion energy, cohesive energy, chemical potential, electronic DOS, and charge transfer between C<sub>n</sub> and Ni<sub>55</sub>. This material is available free of charge via the Internet at <http://pubs.acs.org>.

## ■ AUTHOR INFORMATION

### Corresponding Author

\*E-mail: chenyuan@ntu.edu.sg.

## ■ ACKNOWLEDGMENT

We acknowledge financial support by AcRF Tier 2 (ARC 13/07) from the Ministry of Education, Singapore, and CRP (NRF-CRP2-2007-02) and POC (NRF2010-POC001-021) from the National Research Foundation, Singapore.

## ■ REFERENCES

- (1) Bachilo, S. M.; Balzano, L.; Herrera, J. E.; Pompeo, F.; Resasco, D. E.; Weisman, R. B. Narrow (n,m)-Distribution of Single-Walled Carbon Nanotubes Grown using a Solid Supported Catalyst. *J. Am. Chem. Soc.* **2003**, *125*, 11186–11187.
- (2) Ding, L.; Tselev, A.; Wang, J. Y.; Yuan, D. N.; Chu, H. B.; McNicholas, T. P.; Li, Y.; Liu, J. Selective Growth of Well-Aligned Semiconducting Single-Walled Carbon Nanotubes. *Nano Lett.* **2009**, *9*, 800–805.
- (3) Ciuparu, D.; Chen, Y.; Lim, S.; Haller, G. L.; Pfefferle, L. Uniform-Diameter Single-Walled Carbon Nanotubes Catalytically Grown in Cobalt-Incorporated MCM-41. *J. Phys. Chem. B* **2004**, *108*, 503–507.
- (4) Li, X. L.; Tu, X. M.; Zaric, S.; Welsher, K.; Seo, W. S.; Zhao, W.; Dai, H. J. Selective Synthesis Combined with Chemical Separation of Single-Walled Carbon Nanotubes for Chirality Selection. *J. Am. Chem. Soc.* **2007**, *129*, 15770–15571.
- (5) Chiang, W. H.; Sankaran, R. M. Linking Catalyst Composition to Chirality Distributions of as-Grown Single-Walled Carbon Nanotubes by Tuning Ni<sub>x</sub>Fe<sub>1-x</sub> Nanoparticles. *Nat. Mater.* **2009**, *8*, 882–886.
- (6) Charlier, J. C.; DeVita, A.; Blase, X.; Car, R. Microscopic Growth Mechanisms for Carbon Nanotubes. *Science* **1997**, *275*, 646–649.
- (7) Kwon, Y. K.; Lee, Y. H.; Kim, S. G.; Jund, P. Morphology and Stability of Growing Multiwall Carbon Nanotubes. *Phys. Rev. Lett.* **1997**, *79*, 2065–2068.
- (8) Page, A. J.; Ohta, Y.; Okamoto, Y.; Irle, S.; Morokuma, K. Defect Healing during Single-Walled Carbon Nanotube Growth: A Density-Functional Tight-Binding Molecular Dynamics Investigation. *J. Phys. Chem. C* **2009**, *113*, 20198–20207.
- (9) Irle, S.; Ohta, Y.; Okamoto, Y.; Page, A. J.; Wang, Y.; Morokuma, K. Milestones in Molecular Dynamics Simulations of Single-Walled Carbon Nanotube Formation: A Brief Critical Review. *Nano Res.* **2009**, *2*, 755–767.

- (10) Reich, S.; Li, L.; Robertson, J. Control the Chirality of Carbon Nanotubes by Epitaxial Growth. *Chem. Phys. Lett.* **2006**, *421*, 469–472.
- (11) Ding, F.; Larsson, P.; Larsson, J. A.; Ahuja, R.; Duan, H. M.; Rosen, A.; Bolton, K. The Importance of Strong Carbon–Metal Adhesion for Catalytic Nucleation of Single-Walled Carbon Nanotubes. *Nano Lett.* **2008**, *8*, 463–468.
- (12) Ding, F.; Harutyunyan, A. R.; Yakobson, B. I. Dislocation Theory of Chirality-Controlled Nanotube Growth. *Proc. Natl. Acad. Sci. U.S.A.* **2009**, *106*, 2506–2509.
- (13) Helveg, S.; Lopez-Cartes, C.; Sehested, J.; Hansen, P. L.; Clausen, B. S.; Rostrup-Nielsen, J. R.; Abild-Pedersen, F.; Norskov, J. K. Atomic-Scale Imaging of Carbon Nanofibre Growth. *Nature* **2004**, *427*, 426–429.
- (14) Sharma, R.; Iqbal, Z. In Situ Observations of Carbon Nanotube Formation using Environmental Transmission Electron Microscopy. *Appl. Phys. Lett.* **2004**, *84*, 990–992.
- (15) Hofmann, S.; Sharma, R.; Ducati, C.; Du, G.; Mattevi, C.; Cepek, C.; Cantoro, M.; Pisana, S.; Parvez, A.; Cervantes-Sodi, F.; In Situ Observations of Catalyst Dynamics during Surface-Bound Carbon Nanotube Nucleation. *Nano Lett.* **2007**, *7*, 602–608.
- (16) Hubig, S. M.; Lindeman, S. V.; Kochi, J. K. Charge-Transfer Bonding in Metal–Arene Coordination. *Coordin. Chem. Rev.* **2000**, *200*, 831–873.
- (17) Wang, Q.; Ng, M. F.; Yang, S. W.; Yang, Y. H.; Chen, Y. A. The Mechanism of Single-Walled Carbon Nanotube Growth and Chirality Selection Induced by Carbon Atom and Dimer Addition. *ACS Nano* **2010**, *4*, 939–946.
- (18) Zhang, Y.; Li, Y.; Kim, W.; Wang, D.; Dai, H. Imaging As-Grown Single-Walled Carbon Nanotubes Originated from Isolated Catalytic Nanoparticles. *Appl. Phys. A: Mater. Sci. Process.* **2002**, *74*, 325–328.
- (19) Nasibulin, A. G.; Pikhitsa, P. V.; Jiang, H.; Kauppinen, E. I. Correlation Between Catalyst Particle and Single-Walled Carbon Nanotube Diameters. *Carbon* **2005**, *43*, 2251–2257.
- (20) Zhu, W. M.; Rosen, A.; Bolton, K. Changes in Single-Walled Carbon Nanotube Chirality During Growth and Regrowth. *J. Chem. Phys.* **2008**, *128*, 124708.
- (21) Borjesson, A.; Zhu, W. M.; Amara, H.; Bichara, C.; Bolton, K. Computational Studies of Metal–Carbon Nanotube Interfaces for Regrowth and Electronic Transport. *Nano Lett.* **2009**, *9*, 1117–1120.
- (22) Wang, Q. A.; Lim, K. H.; Yang, S. W.; Yang, Y. H.; Chen, Y. A. Atomic Carbon Adsorption on Ni Nanoclusters: A DFT Study. *Theor. Chem. Acc.* **2011**, *128*, 17–24.
- (23) Brinkmann, G.; Fowler, P. W.; Manolopoulos, D. E.; Palser, A. H. R. A Census of Nanotube Caps. *Chem. Phys. Lett.* **1999**, *315*, 335–347.
- (24) Lair, S. L.; Herndon, W. C.; Murr, L. E.; Quinones, S. A. End Cap Nucleation of Carbon Nanotubes. *Carbon* **2006**, *44*, 447–455.
- (25) Reich, S.; Li, L.; Robertson, J. Structure and Formation Energy of Carbon Nanotube Caps. *Phys. Rev. B: Condens. Matter* **2005**, *72*, 165423.
- (26) Ohta, Y.; Okamoto, Y.; Page, A. J.; Irle, S.; Morokuma, K. Quantum Chemical Molecular Dynamics Simulation of Single-Walled Carbon Nanotube Cap Nucleation on an Iron Particle. *ACS Nano* **2009**, *3*, 3413–3420.
- (27) Zhu, W. M.; Borjesson, A.; Bolton, K. DFT and Tight Binding Monte Carlo Calculations Related to Single-Walled Carbon Nanotube Nucleation and Growth. *Carbon* **2010**, *48*, 470–478.
- (28) Fukui, K. Role of Frontier Orbitals in Chemical Reaction. *Science* **1982**, *218*, 747–754.
- (29) Fukui, K. The Role of Frontier Orbital in Chemical Reactions (Nobel Lectures). *Angew. Chem., Int. Ed. Engl.* **1982**, *21*, 801–809.
- (30) Lee, Y. H.; Kim, S. G.; Tomanek, D. Catalytic Growth of Single-Wall Carbon Nanotubes: An Ab Initio Study. *Phys. Rev. Lett.* **1997**, *78*, 2393–2396.
- (31) Kumeda, Y.; Fukuhiro, Y.; Taketsugu, T.; Hirano, T. Theoretical Study of Nanotube Growth in Terms of Frontier Density Distribution. *Chem. Phys. Lett.* **2001**, *333*, 29–35.
- (32) Hossain, M. Z. Structural Instability of Single Wall Carbon Nanotube Edges from First Principles. *Appl. Phys. Lett.* **2009**, *95*, 153104.
- (33) Anisimov, A. S.; Nasibulin, A. G.; Jiang, H.; Launois, P.; Cambedouzou, J.; Shandakov, S. D.; Kauppinen, E. I. Mechanistic Investigations of Single-Walled Carbon Nanotube Synthesis by Ferrocene Vapor Decomposition in Carbon Monoxide. *Carbon* **2010**, *48*, 380–388.
- (34) Lin, M.; Tan, J. P. Y.; Boothroyd, C.; Loh, K. P.; Tok, E. S.; Foo, Y. L. Direct Observation of Single-Walled Carbon Nanotube Growth at the Atomistic Scale. *Nano Lett.* **2006**, *6*, 449–452.
- (35) Yoshida, H.; Takeda, S.; Uchiyama, T.; Kohno, H.; Homma, Y. Atomic-Scale In Situ Observation of Carbon Nanotube Growth from Solid State Iron Carbide Nanoparticles. *Nano Lett.* **2008**, *8*, 2082–2086.
- (36) Yao, Y. G.; Feng, C. Q.; Zhang, J.; Liu, Z. F. “Cloning” of Single-Walled Carbon Nanotubes via Open-End Growth Mechanism. *Nano Lett.* **2009**, *9*, 1673–1677.
- (37) Yu, X. C.; Zhang, J.; Choi, W.; Choi, J. Y.; Kim, J. M.; Gan, L. B.; Liu, Z. F. Cap Formation Engineering: From Opened C<sub>60</sub> to Single-Walled Carbon Nanotubes. *Nano Lett.* **2010**, *10*, 3343–3349.
- (38) Perdew, J. P.; Burke, K.; Ernzerhof, M. Generalized Gradient Approximation Made Simple. *Phys. Rev. Lett.* **1996**, *77*, 3865.
- (39) Kresse, G.; Furthmüller, J. Efficiency of Ab-Initio Total Energy Calculations for Metals and Semiconductors using a Plane-wave Basis Set. *Comput. Mater. Sci.* **1996**, *6*, 15–50.
- (40) Kresse, G.; Furthmüller, J. Efficient Iterative Schemes for Ab Initio Total-Energy Calculations Using a Plane-Wave Basis Set. *Phys. Rev. B* **1996**, *54*, 11169–11186.
- (41) Blöchl, P. E. Projector Augmented-Wave Method. *Phys. Rev. B* **1994**, *50*, 17953.
- (42) Kresse, G.; Joubert, D. From Ultrasoft Pseudopotentials to the Projector Augmented-Wave Method. *Phys. Rev. B* **1999**, *59*, 1758.
- (43) Bader, R. F. *Atoms in Molecules: A Quantum Theory*; Oxford University Press: Oxford, U.K., 1994.
- (44) Sanville, E.; Kenny, S. D.; Smith, R.; Henkelman, G. Improved Grid-Based Algorithm for Bader Charge Allocation. *J. Comput. Chem.* **2007**, *28*, 899–908.
- (45) Henkelman, G.; Arnaldsson, A.; Jonsson, H. A Fast and Robust Algorithm for Bader Decomposition of Charge Density. *Comput. Mater. Sci.* **2006**, *36*, 354–360.
- (46) Becke, A. D.; Edgecombe, K. E. A Simple Measure of Electron Localization in Atomic and Molecular Systems. *J. Chem. Phys.* **1990**, *92*, 5397–5403.
- (47) Savin, A.; Jepsen, O.; Flad, J.; Andersen, O. K.; Preuss, H.; Vonschnering, H. G. Electron Localization in Solid-State Structures of the Elements — The Diamond Structure. *Angew. Chem., Int. Ed. Engl.* **1992**, *31*, 187–188.

## **Supporting Information**

### **Charge Transfer between Metal Clusters and Growing Carbon Structures in Chirality-Controlled Single-Walled Carbon Nanotube Growth**

Qiang Wang,<sup>†</sup> Shuo-Wang Yang,<sup>‡</sup> Yanhui Yang,<sup>†</sup> Mary B. Chan-Park,<sup>†</sup> and Yuan Chen<sup>†,\*</sup>

<sup>†</sup>School of Chemical and Biomedical Engineering, Nanyang Technological University, 62 Nanyang Drive, Singapore 637459; and <sup>‡</sup>Institute of High Performance Computing, 1 Fusionopolis Way, no. 16-16 Connexis, Singapore 138632, Singapore

\*Corresponding E-mail: chenyuan@ntu.edu.sg

(1) Adhesion energies of C <sub>n</sub> on Ni <sub>55</sub>	S2
(2) Cohesive energies of C–C and C–Ni in Ni <sub>55</sub> –C <sub>n</sub> complexes	S5
(3) Chemical potentials of C <sub>n</sub> on Ni <sub>55</sub>	S7
(4) Charge transfer (or redistribution) between C <sub>n</sub> and Ni <sub>55</sub>	S10
(5) Electronic DOS of edge carbon atoms	S13
(6) References	S16

### (1) Adhesion energy of C<sub>n</sub> on Ni<sub>55</sub>:

The total adhesion energy of carbon structures (C<sub>n</sub>) on the Ni<sub>55</sub> cluster was defined by the energy difference between the fully geometry-optimized Ni<sub>55</sub>-C<sub>n</sub> complex and the corresponding separated Ni<sub>55</sub> and C<sub>n</sub>:

$$E_{T(C-Ni)} = E_{Ni_{55}-C_n} - (E_{Ni_{55}} + E_{C_n}) \quad (1)$$

The total adhesion energies of C<sub>n</sub> structures on the Ni<sub>55</sub> cluster for both armchair (5,5), chiral (6,5), and zigzag (9,0) nanotubes at different growth stages are shown in Figure S2. They span from about 5 to 22 eV. The adhesion energies change significantly at the cap nucleation stages. It is generally considered that the nucleation and formation of chiral caps are critical in deciding the chirality of SWCNTs.<sup>1, 2</sup> At initial nucleation step, small carbon species are key intermediates interacting with metal clusters. Single carbon atoms have stronger adsorption on surface hollow sites (6.94 eV/C for the fcc site and 7.09 eV/C for the hcp site), and they can penetrate the Ni cluster (7.34 eV/C for the tetrahedral subsurface site (tss) and 7.41 eV/C for the octahedral subsurface site (oss)). The activation energy barrier is about 0.25 eV for an adsorbed surface carbon atom to migrate from the fcc hollow site to the underneath oss subsurface site.<sup>3</sup> However, we found that C<sub>2</sub> dimers and C<sub>3</sub> chains, as small elementary units for SWCNT growth, are unable to penetrate the Ni<sub>55</sub> cluster, and they can only adsorb on the cluster surface (7.06 eV/C for C<sub>2</sub> dimers and 5.75 eV/C for C<sub>3</sub> chains). This may be because of fact that their relative weak interaction with Ni atoms and strong covalent bonds among carbon atoms. These results suggest that carbon structure growth happens on the surface of metal clusters, even though single carbon atoms could initially penetrate clusters.

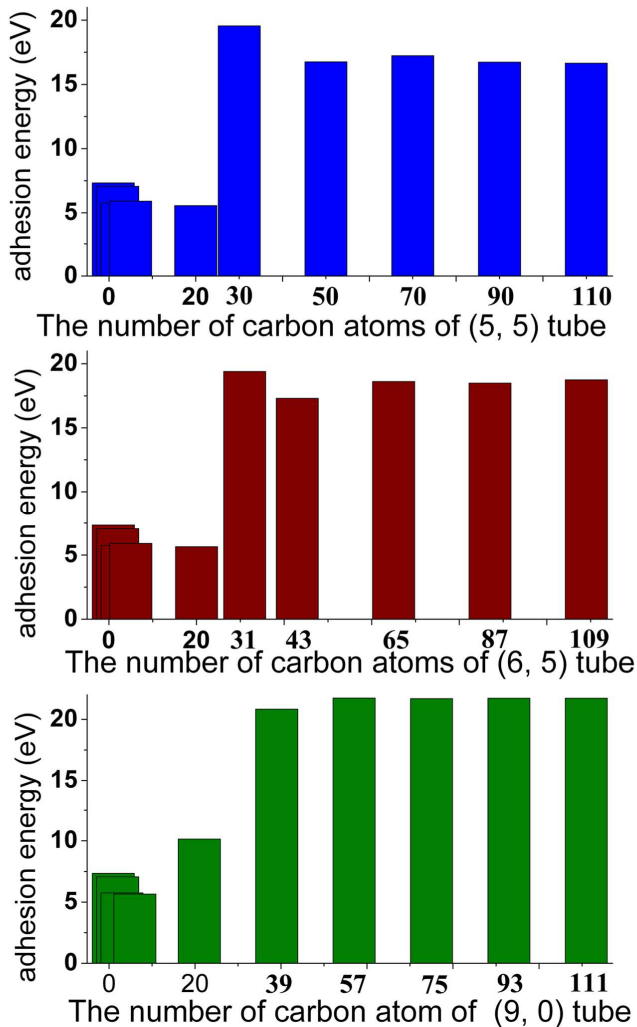


**Figure S1.** The total adhesion energies of  $C_n$  structures on the  $Ni_{55}$  cluster at different growth stages for armchair (5,5), chiral (6,5), and zigzag (9,0) nanotubes. The carbon atom number corresponds to the carbon number in various carbon structures as sketched in the main text Figure 1.

In the following steps of chiral cap formation, small carbon species would first coalesce into five or six-membered carbon rings. The five-membered carbon ring, attached on the surface of the  $Ni_{55}$  cluster (Figure 1B (a)), has adhesion energy of 5.91 eV,

which is 0.26 eV higher than that of the six-membered carbon ring attached on the same Ni<sub>55</sub> cluster (Figure 1B (f)). This agrees with results from first-principle calculations<sup>4</sup> and molecular simulations,<sup>5</sup> which suggests the preferential formation of five-membered carbon rings over six-membered carbon rings on metal clusters during the chiral cap formation. Subsequently, the intermediate cap fragment (Figure 1B (b), Ni<sub>55</sub>C<sub>20</sub>) has a smaller adhesion energy of 5.56 eV. The strongest adhesion energy in the growth of (5,5) nanotube exists when a complete (5,5) end cap (Figure 1B (c), Ni<sub>55</sub>–(5,5) Cap) is formed. Similarly, in the growth of (9,0) nanotube, the adhesion energy is 4.59 eV for creating the intermediate cap fragment (Figure 1B (g), Ni<sub>55</sub>C<sub>21</sub>). This is much lower compared with the adhesion energy of 20.82 eV, when the complete (9,0) cap (Figure 1B (h), Ni<sub>55</sub>–(9,0) Cap) is produced. For the (6,5) nanotube, the first few steps are the same as those of the (5,5) nanotubes. And the adhesion energy of the complete (6,5) cap (Figure 1B (e)) is slightly smaller than that of the intermediate cap fragment Ni<sub>55</sub>C<sub>31</sub> (Figure 1B (d)). Please note that complete caps have been lifted from the Ni<sub>55</sub> cluster surface, and only end edge carbon atoms of the caps are attached on the Ni<sub>55</sub> cluster surface.

A chiral carbon cap can sequentially grow into the corresponding (*n,m*) SWCNT by continuous addition of C<sub>2</sub> dimers at the interface between chiral cap/nanotube ends and the Ni<sub>55</sub> cluster. The growth energies of (5,5), (6,5), and (9,0) nanotubes differ maximum by only a couple of eV throughout the growth from the complete chiral caps. The (5,5), (6,5), and (9,0) nanotubes have adhesion energies of 17.00 ± 0.25, 18.60 ± 0.15 and 21.70 ± 0.10 eV, respectively. The zigzag (9,0) nanotube has larger adhesion energies than those of armchair (5,5) and chiral (6,5) nanotubes. It has been proposed the chirality selection in SWCNT growth could be influenced by the adhesion energy between

growing nanotube structures and metal clusters.<sup>6</sup> However, the optimal strengths required for SWCNT growth between carbon and carbon or between carbon and metal are still unclear. To gain a better understanding on their interaction strengths, in this study, we further examined the evolution of C–C and C–Ni interactions throughout the nanotube growth.

## (2) Cohesive energies of C–C and C–Ni in Ni<sub>55</sub>–C<sub>n</sub> complexes:

The average cohesive energy of C–Ni per C atom of Ni<sub>55</sub>–C<sub>n</sub> complexes was calculated by dividing the total adhesion energy by the number of C atoms (n) adsorbed on the Ni<sub>55</sub> cluster.

$$E_{C-Ni} = E_{T(C-Ni)} / n \quad (2)$$

The cohesive energy of C–C (EC–C ) of C<sub>n</sub> on Ni<sub>55</sub> was estimated by the following procedure: first, the final optimized geometry of the corresponding Ni<sub>55</sub>–C<sub>n</sub> complex was fixed; then all Ni atoms were taken away; and lastly, a single point calculation was performed to obtain the energy ( $E_{C_n}$ ) matching to the remaining C<sub>n</sub> structure. EC–C is calculated by the equation:

$$E_{C-C} = (nE_C - E_{C_n}) / n \quad (3)$$

where  $E_C$  is the energy of a free carbon atom at its ground state, 7.7 eV.<sup>7</sup>

Figure S2 summarizes cohesive energies of C–C and C–Ni interactions per carbon atom for growing armchair (5,5), chiral (6,5), and zigzag (9,0) Ni<sub>55</sub>–C<sub>n</sub> complexes. It shows the changing trend of C–C interactions is opposite to that of C–Ni interactions. For various C<sub>n</sub> structures, the cohesive energy of C–C per carbon atom is weaker at the

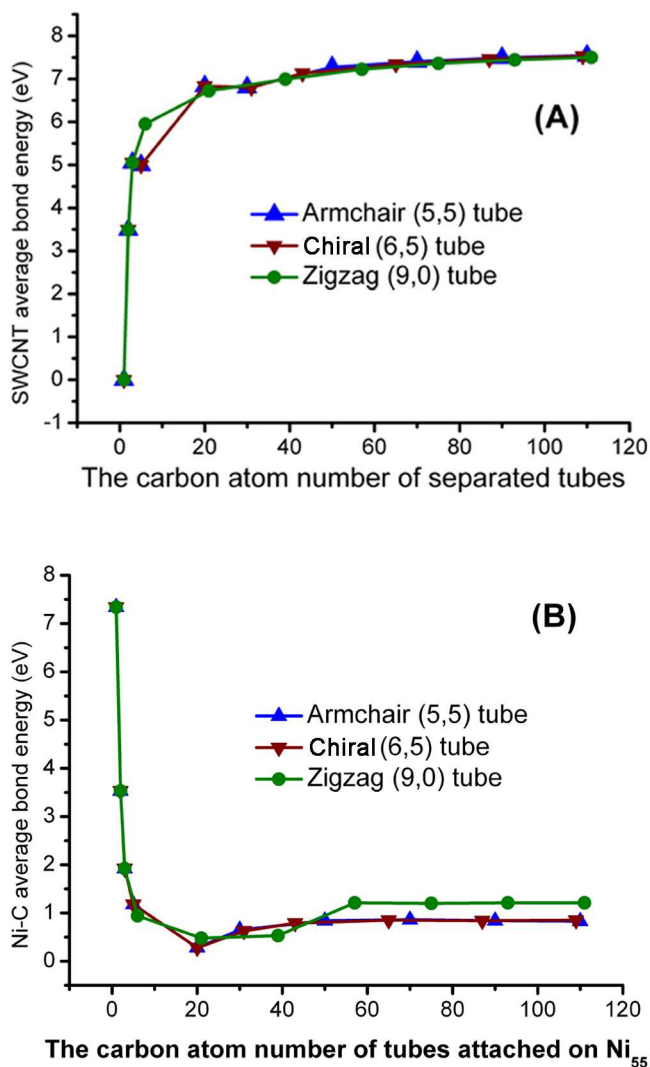


**Figure S2.** (A) The average C–C interaction energies per atom, and (B) the average C–Ni interaction energies per atom for growing armchair (5,5), chiral (6,5), and zigzag (9,0)  $\text{Ni}_{55}\text{--C}_n$  complexes. The number of carbon atoms corresponds to models illustrated in the main text Figure 1.

beginning, and then, it increases rapidly with the expansion of  $\text{C}_n$ , until complete chiral caps are formed. Subsequently, the C–C energy would only increase slightly to about 7.50 eV/C. For the (5,5), (6,5), and (9,0) nanotubes, once chiral caps are formed, there are

no significant changes in their C–C interaction strengths with the elongation of nanotubes. On the opposite, the cohesive energy of C–Ni per carbon atom is strong (about 7.20 eV/C) at the start. Then, it decrease rapidly until the formation of complete chiral caps on the Ni<sub>55</sub> cluster surface. At last, the C–Ni interaction energy shows minimum changes with the nanotube growth. These results suggest there is a competition among the interactions of C–C, C–Ni and Ni–Ni throughout the growth of SWCNTs. Their strengths would adjust continuously with the growth of C<sub>n</sub> on metal clusters until reaching an equilibrium during the extension of nanotube length.

### **(3) Chemical potential of C<sub>n</sub> on Ni<sub>55</sub>:**

Chemical potential ( $\mu$ ) of the growing carbon structure (C<sub>n</sub>) on Ni<sub>55</sub>, which is the energy required to add one extra carbon atom during SWCNT growth, was defined as:

$$\mu = \frac{E_{\text{Ni}_{55}-C_n} - E_{\text{Ni}_{55}}}{n} - \mu_c \quad (4)$$

where  $E_{\text{Ni}_{55}-C_n}$  and  $E_{\text{Ni}_{55}}$  are the total energies of fully geometry-optimized complexes with and without C<sub>n</sub>, respectively. n corresponds to the number of carbon atoms in C<sub>n</sub>. The reference chemical potential,  $\mu_c$ , is the chemical potential of a free carbon atom at its ground state, 7.7 eV. Chemical potential has previously been applied in SWCNT nucleation and growth studies.<sup>7</sup>

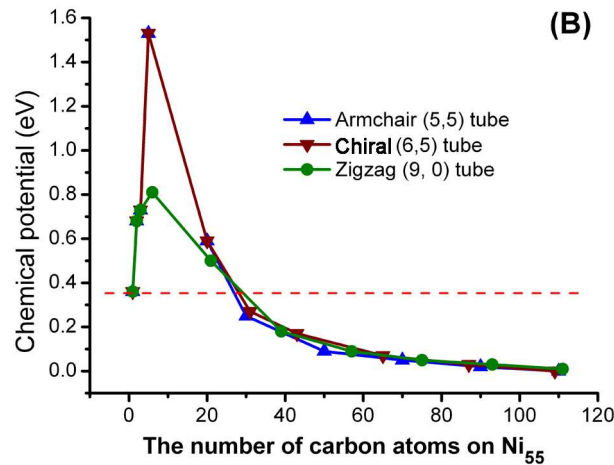
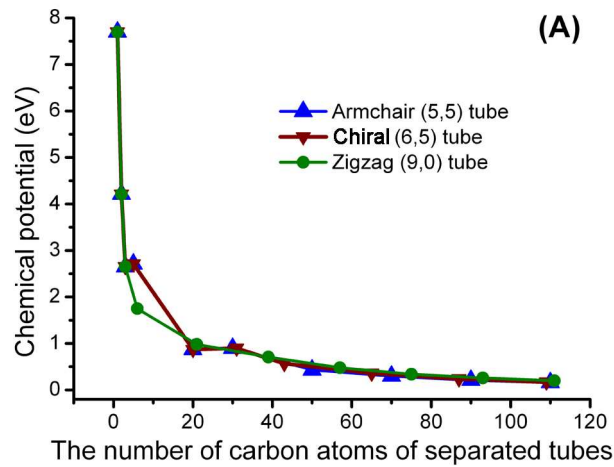


**Figure S3.** Chemical potentials of various carbon structures: (A)  $C_n$  without metal clusters, and (B)  $Ni_{55}-C_n$  complexes of (5,5), (6,5), and (9,0) nanotubes. The chemical potentials are expressed with respect to the chemical potential of a free carbon atom in its ground state. The number of carbon atoms corresponds to models sketched in the main text Figure 1.

The energy needed to add one extra carbon atom to a  $C_n$  is defined as its chemical potential ( $\mu$ ). Figure S3 show chemical potentials of various possible  $C_n$  structures

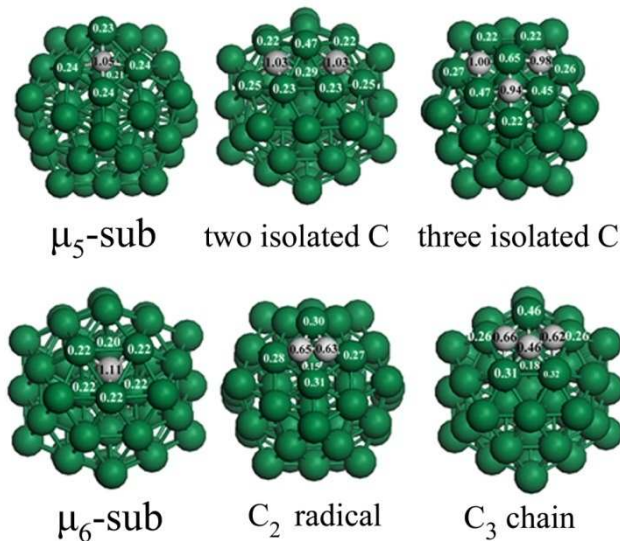
(illustrated in Figure 1), which could appear in the process of growing (5,5), (6,5), and (9,0) nanotubes. First, we studied the growth of these  $C_n$  without metal clusters. Shown in Figure S4A, the chemical potentials of  $C_n$  decline rapidly until complete (5,5), (6,5), or (9,0) carbon caps are formed. Subsequently, they decrease gradually to zero with the increase of nanotube lengths. The result suggests that carbon atoms can spontaneously assemble into carbon caps leading to nanotube growth under catalyst-free condition. However, significant differences are observed when these  $C_n$  structures are grown on the  $Ni_{55}$  cluster. During initial nucleation, the adsorption of single carbon atoms on various surface sites of the  $Ni_{55}$  cluster (0.76 eV at fcc site and 0.61 eV at hcp site) has higher chemical potentials than the adsorption at subsurface sites (0.36 eV at oss site and 0.29 eV at tss site). Note that only the chemical potential at the subsurface oss site is shown on Figure S4B. Moreover, chemical potentials of a  $C_2$  dimer and a  $C_3$  chain adsorbed on the  $Ni_{55}$  cluster surface sites are 0.68 and 0.73 eV, respectively, which are higher than that of single carbon atom at subsurface sites. These results imply that single carbon atom would rather penetrate the  $Ni_{55}$  cluster than stay on the surface or form  $C_2/C_3$ . This is consistent with our previous transition state calculation.<sup>3</sup> During the formation of chiral caps, the five-membered carbon ring has the highest chemical potential over all SWCNT growth stages at 1.53 eV. The six-membered carbon ring has the second highest chemical potential at 0.81 eV. The high chemical potentials of carbon rings have two implications: (1) considering the lower chemical potentials of  $C/C_2/C_3$  species, it suggests that C species at low coverage on metal surface would not spontaneously assemble into carbon rings. The formation of five- and six-membered carbon rings requires a large surface coverage of carbon species with chemical potentials exceeding 1.53 eV or 0.81 eV, in

agreement with a recent paper.<sup>7</sup> (2) Once these small carbon rings are formed under certain surface coverage of carbon species, they can spontaneously extend into larger carbon structures by incorporating more small carbon species, because chiral cap intermediates ( $C_{20}$ ,  $C_{21}$ , and  $C_{22}$ ) and complete (5,5), (6,5), and (9,0) chiral caps all have lower chemical potentials than those of carbon rings on the  $Ni_{55}$  cluster. During the growth of chiral nanotubes, the growing nanotubes have lower chemical potentials than small carbon species (under the red line indicated on Figure S4B), and their chemical potentials would decrease gradually to zero with the increase of nanotube length. It suggests that complete chiral carbon caps, attached on the metal cluster, would spontaneously grow into nanotubes by incorporating other carbon species adsorbed on the metal surface. Furthermore, the chemical potentials of all  $C_n$  structures attached on the metal cluster are lower than those of corresponding  $C_n$  structures in gas phase. This implies that the adsorption of  $C_n$  structures on metal clusters is energetically favored. It also suggests there is a driving force from dissociation of carbon species in gas phase toward adsorption of carbon species on metal clusters and growth of carbon structures.

#### **(4) Charge transfer (or redistribution) between $C_n$ and $Ni_{55}$ :**

Based on the above energy calculation results, the growth energies of (5,5), (6,5), and (9,0) nanotubes differ by only a couple of eV, considering the high growth temperature, which implies no strong preference for specific chirality. A recent theoretical study concluded that free metal clusters are incapable to grow SWCNTs with a desired chirality, and the cluster engineering is not a promising method for chirality controlled SWCNT production,<sup>7</sup> which is not in agreement with the existing experimental

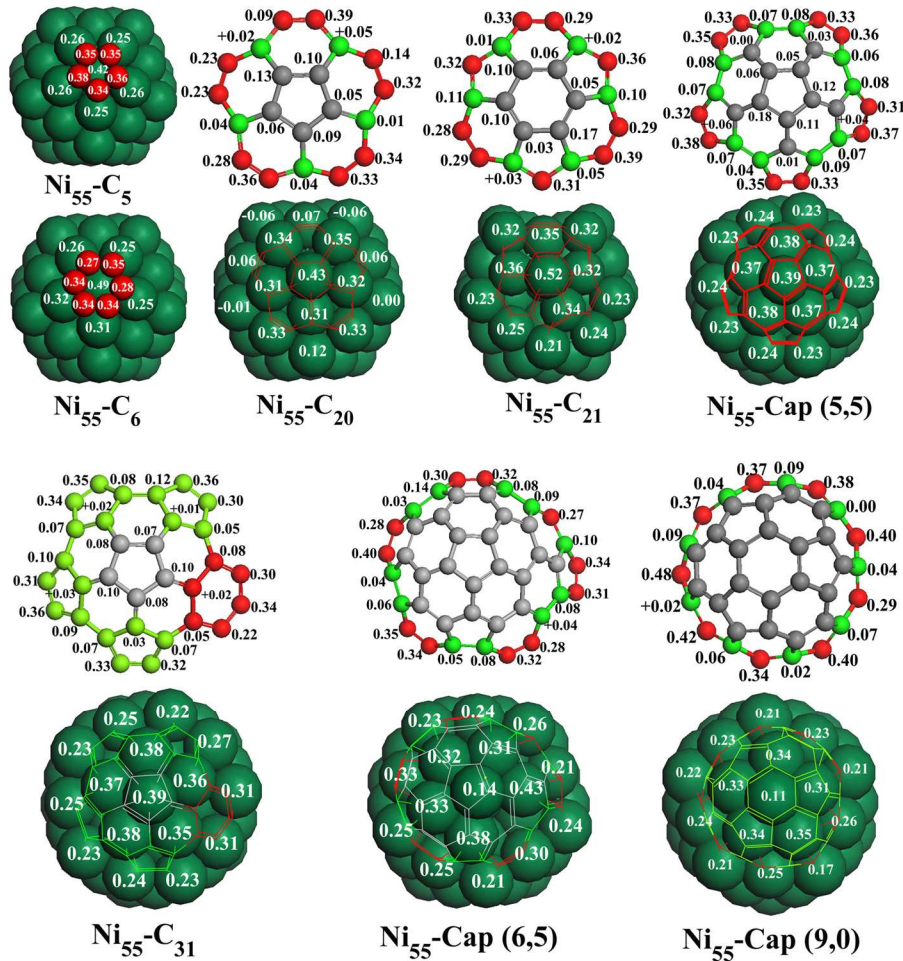
results. Something seems missing in the energy consideration alone. To reveal the hidden role of metal clusters in chirality-controlled SWCNT growth, the charge population at the boundary between carbon structures ( $C_n$ ) and the  $Ni_{55}$  cluster was studied using the atomic Bader charge analysis.



**Figure S4.** Charge distribution of small carbon species adsorbed on the  $Ni_{55}$  cluster.

As shown in Figure S4, during the initial nucleation, individual carbon atoms hold larger negative charges (about  $-1.00$  e/C) than those of  $C_2$  dimers or  $C_3$  chains (about  $-0.60$  e/C). During the formation of chiral caps, the five- and six-membered rings have the lowest negative charge (about  $-0.35$ e/C), shown on Figure S6. The dramatic charge redistribution in the growing carbon structures from individual carbon atoms to carbon rings may be because of the lateral repulsion among carbon atoms. The Bader charge calculation for the  $Ni_{55}$  cluster indicates that a significant part of negative charges accumulated on carbon atoms is transferred from neighbor Ni atoms. Ni atoms have positive charges spanning from about  $+0.2$  to  $+0.65$  e/Ni. We focused on the charge

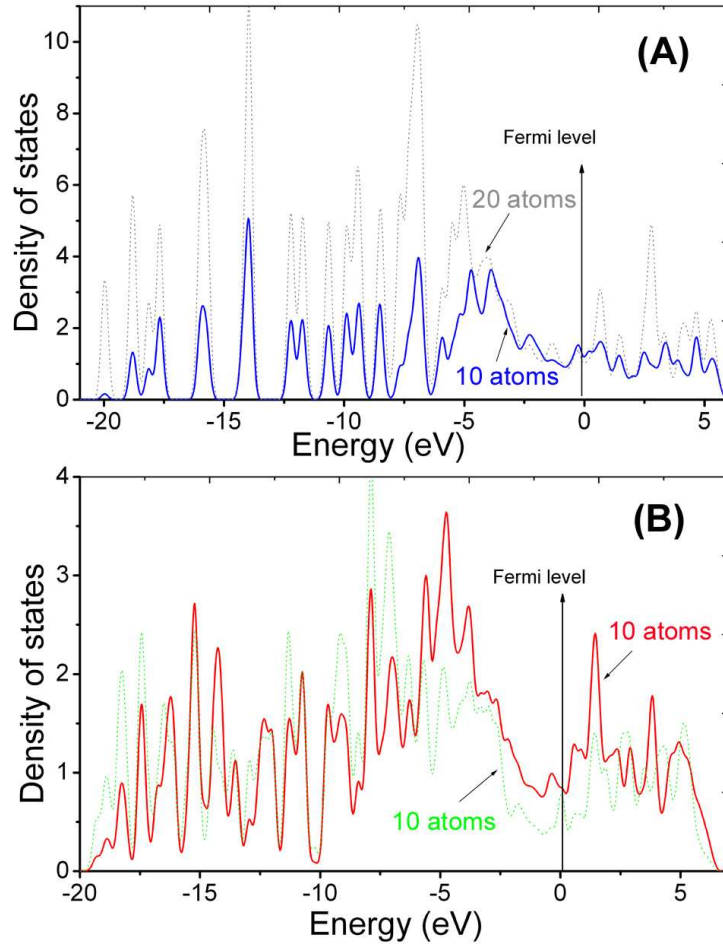
transfer at the interface between growing carbon structure  $C_n$  and the  $Ni_{55}$  cluster to reveal the role of metal clusters in chirality-controlled SWCNT synthesis. We found that negative charges always accumulated on edge atoms of growing carbon structures; in the contrast, the charges of nonedge atoms were close to zero.



**Figure S5.** Charge distribution of carbon rings and cap intermediates on the  $Ni_{55}$  cluster.

The carbon atom number corresponds to models sketched in the main text Figure 1.

**(5) Electronic DOS of edge carbon atoms:**



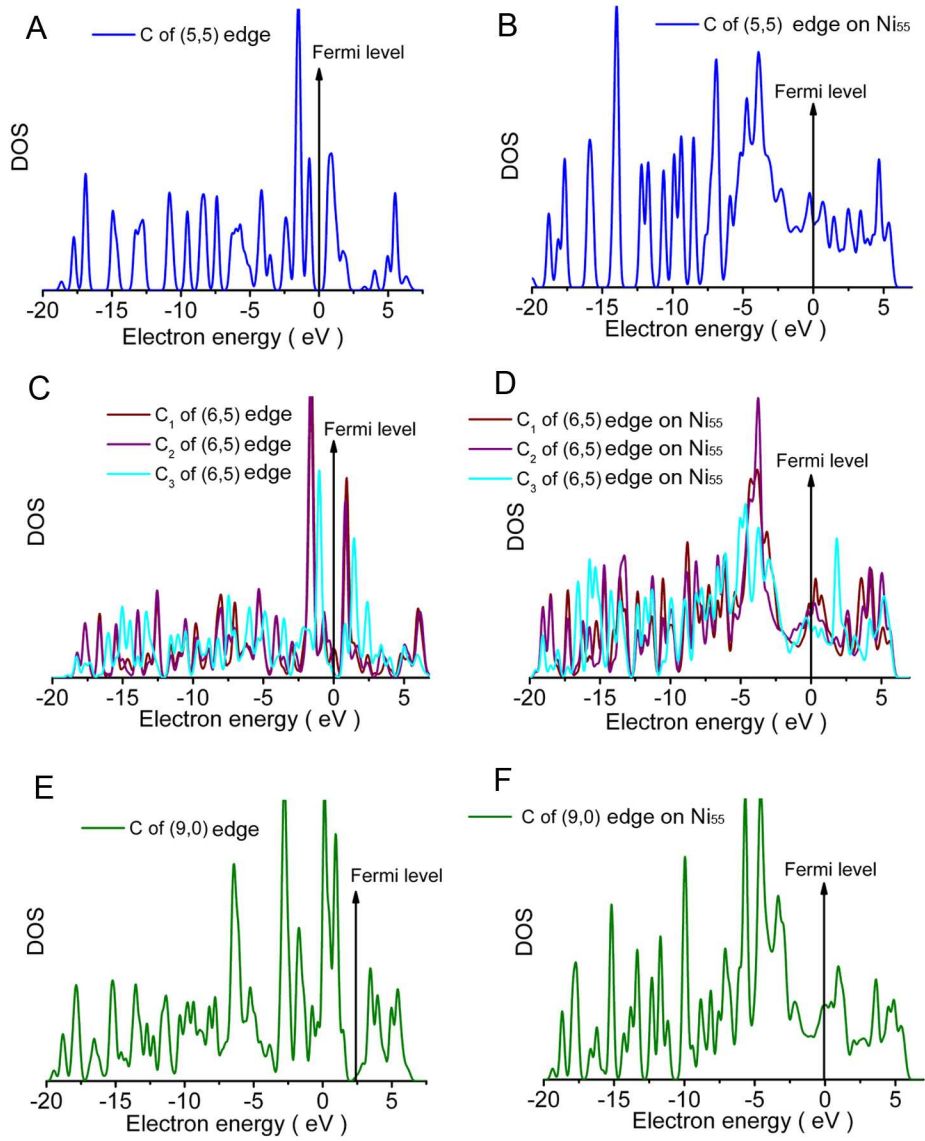
**Figure S6.** DOS of edge carbon atoms: (A) ten outmost edge (blue solid line) and twenty inner (gray dotted line) carbon atoms of the armchair (5,5) cap in the Ni<sub>55</sub>-Cap (5,5) (Figure S1B (c)) complex; (B) five pairs of carbon atoms (highlighted in red on Figure 2C in the main text, red solid line) and other five pairs of carbon atoms (highlighted in green on Figure 2C in the main text, green dotted line) on the Ni<sub>55</sub>-C<sub>110</sub> complex ((Figure S1C (l)). The vertical lines mark the Fermi level of the Ni<sub>55</sub>-Cap (5,5) and the Ni<sub>55</sub>-C<sub>110</sub> complexes, respectively.

Figure S6A shows electronic density of states (DOS) of ten outmost edge carbon

atoms and twenty inner carbon atoms of the armchair (5,5) cap absorbed on the Ni<sub>55</sub> cluster (Ni<sub>55</sub>–Cap (5,5), Figure S1B (c)). The inner carbon atoms dominate core orbitals (< -4.0 eV), whereas the outmost edge atoms have relative small contribution. However, at the frontier orbital region (near the Fermi level), the outmost edge atoms hold about equal electron density as inner carbon atoms. Considering there are only ten outmost edge atoms vs. twenty inner carbon atoms, the equal population of electron density at the frontier orbital region implies the outmost edge carbon atoms are much more reactive than inner carbon atoms.

After the (5,5) cap grows into a (5,5) nanotube, Figure S6B shows the five pairs of outmost carbon atoms with negative charges gained from the metal cluster (highlighted in red on Figure 2C in the main text) are much more reactive than the other five pairs of edge carbon atoms (highlighted in green on Figure 2C in the main text) at the edge of an armchair (5,5) tube in the Ni<sub>55</sub>–C<sub>110</sub> complex ((Figure S1C (l)).

As shown in Figure 5 in the main text, the edge of (5,5) nanotube has ten identical carbon atoms at five pairs of armchair sites; nine identical carbon atoms sit at zigzag sites on the edge of (9,0) nanotube; and the edge of (6,5) nanotube has three carbon atoms at a kink site and eight carbon atoms at four pairs of armchair sites similar to the armchair sites of (5,5) nanotube. We selected five representative edge carbon atoms (one from (5,5) nanotube, one from (9,0) nanotube, and three from the kink site of (6,5) nanotube). Their electronic DOS are shown in Figure S8. Two situations were considered: the first is C<sub>n</sub> structures without metal clusters (Figure S7A, C, E); and the second is nanotubes grown on N<sub>55</sub> (Figure S7 B, D, F).



**Figure S7.** Electronic DOS of five representative carbon atoms: A, C, E, at the edges of (5,5), (6,5), and (9,0) nanotubes without metal clusters; and B, D, F, at boundaries between those nanotubes and Ni<sub>55</sub>.

## (6) References for Supporting Information:

1. Reich, S.; Li, L.; Robertson, J., Structure and Formation Energy of Carbon Nanotube Caps. *Phys. Rev. B: Condens. Matter* **2005**, *72*, 165423.
2. Gomez-Gualdrón, D. A.; Balbuena, P. B., The Role of Cap Chirality in the Mechanism of Growth of Single-Wall Carbon Nanotubes. *Nanotechnol.* **2008**, *19*, 485604.
3. Wang, Q. A.; Lim, K. H.; Yang, S. W.; Yang, Y. H.; Chen, Y. A., Atomic carbon adsorption on Ni nanoclusters: a DFT study. *Theor. Chem. Acc.* **2011**, *128*, 17-24.
4. Fan, X.; Buczko, R.; Puretzky, A. A.; Geohegan, D. B.; Howe, J. Y.; Pantelides, S. T.; Pennycook, S. J., Nucleation of single-walled carbon nanotubes. *Phys. Rev. Lett.* **2003**, *90*, 145501.
5. Ohta, Y.; Okamoto, Y.; Page, A. J.; Irle, S.; Morokuma, K., Quantum Chemical Molecular Dynamics Simulation of Single-Walled Carbon Nanotube Cap Nucleation on an Iron Particle. *Acs Nano* **2009**, *3*, 3413-3420.
6. Ding, F.; Larsson, P.; Larsson, J. A.; Ahuja, R.; Duan, H. M.; Rosen, A.; Bolton, K., The importance of strong carbon-metal adhesion for catalytic nucleation of single-walled carbon nanotubes. *Nano Lett.* **2008**, *8*, 463-468.
7. Zhu, W. M.; Borjesson, A.; Bolton, K., DFT and tight binding Monte Carlo calculations related to single-walled carbon nanotube nucleation and growth. *Carbon* **2010**, *48*, 470-478.